A NORMALIZED PARAMETRIC DOMAIN FOR THE ANALYSIS OF THE LEFT VENTRICULAR FUNCTION

Jaume Garcia-Barnes, Debora Gil
Computer Vision Center, Campus UAB, Bellaterra, Spain

Sandra Pujadas, Francesc Carreras
Hospital de la Sta Creu i St Pau, Barcelona, Spain

Manel Ballester
Department of Cardiology, University of Lleida, Lleida, Spain

Keywords: Helical Ventricular Myocardial Band, Myocardial Fiber, Tagged Magnetic Resonance, HARP, Optical Flow Variational Framework, Gabor Filters, B-Splines.

Abstract: Impairment of left ventricular (LV) contractility due to cardiovascular diseases is reflected in LV motion patterns. The mechanics of any muscle strongly depends on the spatial orientation of its muscular fibers since the motion that the muscle undergoes mainly takes place along the fiber. The helical ventricular myocardial band (HVMB) concept describes the myocardial muscle as a unique muscular band that twists in space in a non homogeneous fashion. The 3D anisotropy of the ventricular band fibers suggests a regional analysis of the heart motion. Computation of normality models of such motion can help in the detection and localization of any cardiac disorder. In this paper we introduce, for the first time, a normalized parametric domain that allows comparison of the left ventricle motion across patients. We address, both, extraction of the LV motion from Tagged Magnetic Resonance images, as well as, defining a mapping of the LV to a common normalized domain. Extraction of normality motion patterns from 17 healthy volunteers shows the clinical potential of our LV parametrization.

1 INTRODUCTION

The Helical Ventricular Myocardial Band (HVMB) concept was developed during the last 50 years by Dr. Torrent-Guasp after more than 1000 anatomical dissections of hearts belonging to different species (Kocica et al., 2006; Torrent-Guasp et al., 2005). His revolutionary (though not fully accepted) theory states that the architecture of the main cavities of the heart arises from the disposition of a unique muscular band in 3D space. This muscular band is twisted in two helical loops from the root of the pulmonary artery to the aorta.

Figure 1 shows the main dissection steps for obtaining the ventricular band of a bovine heart. After unwrapping the myocardial band helical structure, a single straight muscular band is obtained with the pulmonary artery at one side and the aorta at the other (Fig. 1.d). Over this band, four segments are distinguished: right segment (RS), left segment (LS), descendent segment (DS) and ascendent segment (AS)
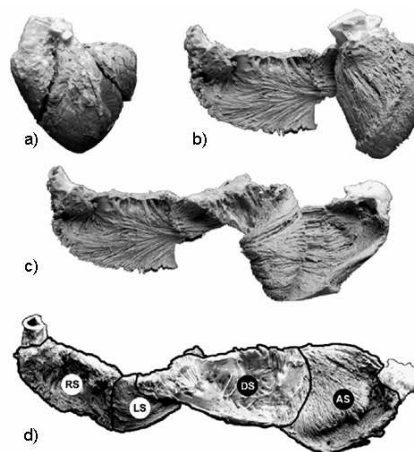

Figure 1: Main steps of the dissection of a bovine heart. Intact myocardium a), myocardial muscle showing the fibers b), unwrapped myocardial band c) and the the four segments of the myocardial band d), which, from left to right, are: right (RS), left (LS), descendent (DS) and ascendent segments (AS). (Photos from (Kocica et al., 2006)).

(Fig. 1.d). The complex spatial distribution of these segments can be appreciated by coloring each of them and wrapping the band again as illustrated in figure 2. The longitudinal (left) and axial (right) views show the complex disposition of the different segments in the myocardium and reveal a highly anisotropic non homogeneous tissue structure.

The contraction mechanics of any muscle strongly depends on the spatial orientation of its muscular fibers since the motion that the muscle undergoes mainly takes place along the fiber (Waldman et al., 1988). Any cardiovascular disease affecting the blood supply at a given myocardial area affects the contractile properties of the ventricular band and, thus, the heart function. It follows that the function and anatomy (given by the ventricular band) of the heart are highly interdependent (Jung et al., 2006; Kocica et al., 2006). The anisotropy in fiber orientation of the ventricular band (fig.2) suggests a regional analysis of the heart motion rather than extracting global scores, such as ejection fraction or wall thickening.

Currently, there are many medical imaging modalities (echo-cardiography, magnetic resonance) that allow assessment of the heart function. Most of them display the myocardium as an homogeneous tissue so that only the outer (epicardium) and inner (endocardium) border dynamics can be appreciated. Although this suffices to compute global scores, extraction of tissue motion within the myocardial walls is not feasible. The only technique that allows noninvasive detailed visualization of the intra-myocardial function is Tagged Magnetic Resonance (TMR) (Zerhouni et al., 1988; Axel and Dougherty, 1989). This technique prints a grid-like pattern of saturated magnetization over the myocardium, which, as it evolves by the underlying motion of tissue, allows visualization of intramural deformation.

Since the appearance of TMR many image processing techniques have been developed in order to obtain vector fields that reflect the functionality of the heart. The techniques developed so far mainly focus on extracting local apparent physical scores (such as strain (Garot et al., 2000; Gotte et al., 2006)) and restoring 3D deformation from 2D TMR projections in order to get more realistic measures of the heart integrity (Li and Denney, 2006; Luo and Heng, 2005). However, few effort has been done towards the computation of normality models for the ventricular function aimed at helping in the detection and localization of cardiac disorders. Up to our knowledge, the only authors addressing computation of motion models are Rao (Rao et al., 2003) and Chandrashekara (Chandrashekara et al., 2003). Their models are designed to add prior information for tracking algorithms and
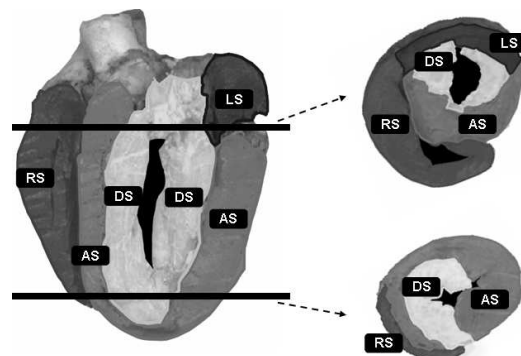

Figure 2: Disposition of the main segments of the band in space by coloring. A longitudinal cut is shown on the left hand-side and two axial cuts from the basal (above) and apical (below) levels are shown on the right hand-side. (Modified and reproduced with kind permission of M. Ballester, Department of Cardiology. University of Lleida. Spain).

are not suitable enough for clinical diagnosis since they discard information prone to discriminate among pathological cases.

In the present work, we introduce a parametric model that characterizes the normal regional motion of the Left Ventricle (LV), appreciated in axial cuts along the systolic cycle. So far, we just focus on basal and apical cuts extracted from 17 healthy volunteers. To obtain this model, two main issues must be addressed first. Computation of the LV dynamics observed in tagged sequences, and definition of a normalized domain for the representation of the LV motion suitable for comparison across patients.

The paper is organized as follows. Our approach to estimation of tissue deformation from TMR sequences is given in Section 2. The normalized domain for computation of normality patterns of the ventricular function is defined in Section 3. In Section 4 we adress the regional analysis of the LV function. In Section 5 we provide the normality models extracted from 17 healthy volunteers. Finally in Section 6 we discuss the research done so far and outline future lines.

2 LEFT VENTRICULAR FUNCTION ESTIMATION

There are many techniques (such as FindTags (Guttman et al., 1994) in spatial domain or HARP (Osman et al., 1999) in Fourier space) addressing computation of LV motion from TMR images. In this paper we use the Harmonic Phase Flow (HPF) method developed by the authors in (Garcia et al., 2006) because it overcomes some of the problems of the above

standard techniques:

- It tracks motion at advance stages of the systolic cycle (like HARP).
- It provides continuous vector fields on the image domain.
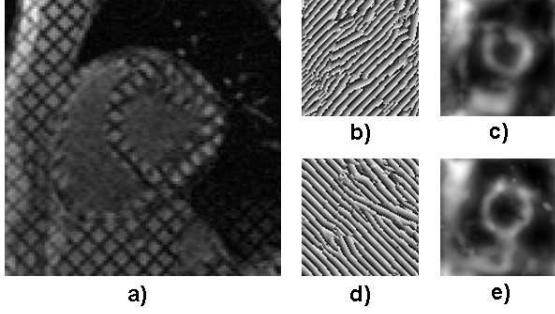- It handles local deformation of tissue.

Figure 3: Given an incoming tagged frame a), two Gabor filter banks are applied to it, leading to a couple of complex images. The wraped version of their phase is shown in b) and d), while their amplitudes in c) and e).
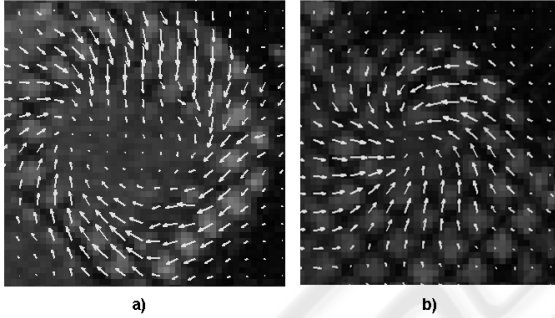

Figure 4: The resultant Harmonic Phase Flow over two analyzed tagged frames, belonging to base a) and apex b).

Let $\{I^t(x,y)\}_{t=0}^{T}$ denote a TMR sequence (fig.3 a)) and $V^t(x,y)$ the vector field matching frames at times t and $t+1$. The HPF estimation of such vector proceeds in two stages: extraction of a representation space capturing local deformations and feature tracking within a variational framework.

The representation space is two dimensional (see fig.3 b) and d)) and is obtained by assigning to each point the maximum response of two Gabor filter banks (one for each tag direction). The Gabor filters are centered around the main frequency of tags and tuned for each myocardial cut (base and apex). The complex images in the representation space will be noted by (I_1^t, I_2^t) and their phase and amplitude by Φ_k and Λ_k, respectively. On one hand, it can be shown (Osman et al., 1999) that Φ_k (fig.3 b) and d)) is a material property of the tissue that remains constant

along the cardiac cycle. Since the brightness constancy constrain is met, classical optical flow (Horn and Schunck, 1981) can be applied two track both phases. On the other hand, Λ_k (fig.3 b) and d)) provides a measure of the reliability of the phase values detected by the Gabor filter banks.

The variational framework we propose regularizes the deformation field at areas where Λ_k drops. The searched vector field, $V^t(x,y) = (\mathcal{U}^t(x,y), \mathcal{V}^t(x,y))$, should minimize the energy:

$$\underbrace{\int (1-(\alpha_1+\alpha_2)/2)^2 \varepsilon_{reg}^2}_{\text{Regularity}} + \underbrace{\int [\alpha_1^2 \varepsilon_1^2 + \alpha_2^2 \varepsilon_2^2]}_{\text{Matching}} \quad (1)$$

where the matching and the regularizing terms are defined as:

$$\varepsilon_k = \Phi_{kx}\mathcal{U} + \Phi_{ky}\mathcal{V} + \Phi_{kt}$$
$$\varepsilon_{reg} = \|\nabla V\|^2 = \|\nabla \mathcal{U}\|^2 + \|\nabla \mathcal{V}\|^2$$

for $\Phi_{kx}, \Phi_{ky}, \Phi_{kt}$, the partial derivatives of the k-essim phase Φ_k and the weighting functions α_k's given by the amplitudes:

$$\alpha_k = \frac{|\Lambda_k|}{max(|\Lambda_k|)}$$

The solution to the Euler Lagrange equations associated to the functional (1) is obtained by solving the gradient descent scheme:

$$
\begin{aligned}
&\partial \mathcal{U}^t/\partial t(x,y) = \\
&-[(\Phi_x g \Phi_x)\mathcal{U}^t(x,y) + (\Phi_x g \Phi_y)\mathcal{V}^t(x,y) + \Phi_x g \Phi_t \\
&-(1-\alpha)^2 \Delta \mathcal{U}^t(x,y) + 2(1-\alpha)\langle \nabla \alpha, \nabla \mathcal{U}^t(x,y)\rangle] \\
\\
&\partial \mathcal{V}^t/\partial t(x,y) = \\
&-[(\Phi_x g \Phi_y)\mathcal{U}^t(x,y) + (\Phi_y g \Phi_y)\mathcal{V}^t(x,y) + \Phi_y g \Phi_t \\
&-(1-\alpha)^2 \Delta \mathcal{V}^t(x,y) + 2(1-\alpha)\langle \nabla \alpha, \nabla \mathcal{V}^t(x,y)\rangle]
\end{aligned}
\quad (2)
$$

where $\langle \cdot, \cdot \rangle$ denotes the scalar product, ∇ and $\triangle$ stand for the gradient and Laplacian operators and $g = diag(\alpha_1^2, \alpha_2^2)$.

The solution to eq. (2) gives our Harmonic Phase Flow. In (Garcia et al., 2006) we prove that it reaches sub-pixel precision in experimental data. Two instances, for basal and apical views, of its performance are shown in figure 4.

3 NORMALIZED PARAMETRIC DOMAIN

Comparing deformation fields from different sequences requires coping with inter and intra patient
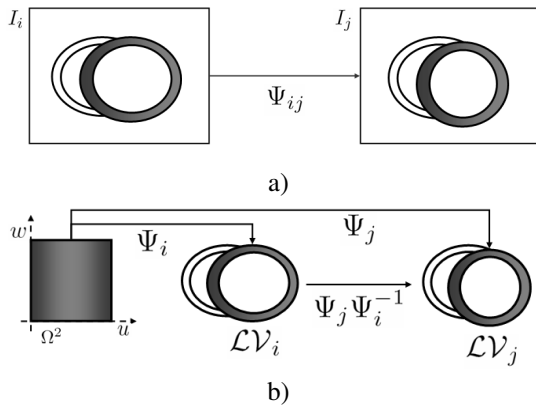
Figure 5: Comparison between image registration and mapping to normalized domain: registration a) and parametrization schemes b).

anatomical variability. In this Section we define a parametrization that maps any left ventricle domain, which we denote by $\mathcal{LV}$, to a common normalized domain, namely $\Omega = [0,1] \times [0,1]$. Such normalized domain allows comparison of different vector fields and, thus, computation of an average model of the $\mathcal{LV}$ functionality. We note that $\mathcal{LV}$ parametrization is an alternative to image registration (Zitova and Flusser, 2003), which maps image sequences to a reference patient. The advantage of our approach is that, besides giving an implicit registration, parametric coordinates provide an intuitive way of moving on the myocardial domain. Figure 5 sketches image registration and $\mathcal{LV}$ parametrization. A registration scheme bases on the mapping, Ψ_{ij}, best matching two images I_i and I_j (fig. 5.a). By using a parametrization, the left ventricles, $\mathcal{LV}_i$ and $\mathcal{LV}_j$, from different sequences, are mapped to the common domain via Ψ_i and Ψ_j and the composition $\Psi_i\Psi_j^{-1}$ registers them (fig. 5.b).

The mapping from the image domain to the parametric domain is done by fitting a bi-dimensional B-Spline over the target left ventricular region. B-Spline fitting splits into fitting the initial spline at time 0 and updating the initial shape under *HPF* deformation.

3.1 Initial Surface Fitting

The LV is a simple geometric entity since it is homeomorphic (it identifies) to a torus. It follows that there are two privileged directions, the circumferential (angular) and the radial. If we parameterize these directions and normalize them in the range $[0,1]$ we obtain a universal (normalized) domain shared by all incoming subjects. We define the initial parametrization, Ψ^0, of the undeformed left ventricular region, $\mathcal{LV}^0$, in 3 stages. First we define a new coordinate system

based on anatomical landmarks in order to account for affine differences among subjects. A B-spline curve fitting of the inner (endocardium) and the outer (epicardium) heart borders defines the angular coordinate. Finally, the radial coordinate is obtained by interpolating values between the two curves using a bi-dimensional spline. The spline modelling accounts for anatomical differences among subjects.

An affine coordinate system is defined by means of an origin of coordinates, O, and two independent axis, V_x, V_y. The new origin is defined as the center of mass of a set of points segmenting the myocardial borders (endocardium and epicardium). By the mechanics of rigid motion it follows that the new origin compensates any translation. The new axis V_x is a unitary vector starting at O and pointing to the point, P_{as}, joining the right (RV) and left ventricles and separating the septum and the anterior walls. Finally the vector V_y is also unitary, orthogonal to V_x and pointing oppositely to the septal wall. By considering the anatomical key point P_{as} as angular origin, we account for any rotational disparity among sequences. Figure 6 describes the new reference system with the key point P_{as} highlighted with a solid black circle.
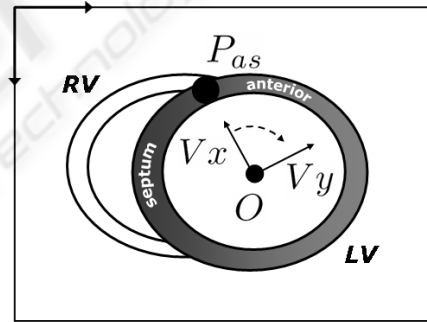

Figure 6: Affine reference accounting for affine transformations across sequences. The image coordinate system is at the upper left corner and the coordinate system based on anatomical features at the $\mathcal{LV}$ center.

Let (x_n^0, y_n^0) and (x_n^1, y_n^1) be, respectively, points on the endocardium and epicardium in the new affine reference. Their angles, θ_n^0 and θ_n^1, serve to fit a pair of closed B-Spline curves, ψ^0, ψ^1, by minimizing:

$$\varepsilon^k = \sum_{n=1}^{N_k} \|\psi^k(\tfrac{\theta_n^k}{2\pi}) - (x_n^k, y_n^k)\|^2 \quad k = 0, 1$$

with

$$\psi^k(u) = \sum_{m=1}^{M_k} R_m^k(u) P_m^k \quad k = 0, 1$$

for R_m^k cubic blending functions and $P_m^k \in \mathbb{R}^2$ control points ensuring a closed curve (i.e. $P_1^k = P_{M_k-2}^k$, $P_2^k = P_{M_k-1}^k$, $P_3^k = P_{M_k}^k$).

In order to get the final parametrization we fit a bi-dimensional spline to a uniform sampling of the radial values (normalized in the range $[0, 1]$) of the two border splines at circumferential parameters $u_i = (i-1)/(Nu-1)$. For each of them we obtain a couple of points belonging to endocardium and epicardium that are also uniformly sampled at radial values $w_j = (j-1)/(Nw-1)$. This provides $N_u \times N_w$ myocardial points, $\{X_{ij}^0\}_{i,j=1}^{N_u,N_w}$, at the initial time. The parametric map is obtained by fitting a bi-dimensional B-Spline surface to such discrete set:

$$\varepsilon = \sum_{i=1}^{N_u} \sum_{j=1}^{N_w} \|\Psi^0(u_i, w_j) - X_{ij}^0\|^2 \qquad (3)$$

with

$$\Psi^0(u, w) = \sum_{n=1}^{M_u} \sum_{m=1}^{M_w} R_n(u) S_m(w) P_{nm}$$

In this case, R_n are cubic blending functions, S_m are quadratic blending functions and $P_{nmj} \in \mathbb{R}^2$ are control points ensuring a closed surface in the angular direction.

3.2 General Surface Fitting

So far we have described the parametrization of the initial left ventricular domain $\mathcal{LV}^0$. We next describe how to parameterize the deformed left ventricular domain, $\mathcal{LV}^t$, at any stage of the systolic cycle ($t > 0$). End systole is defined as the instant where the area of the blood pool inside the LV is minimum. This parametrization is also done by fitting a B-Spline surface over the object of interest. The parametric domain Ω is uniformly sampled in a $N_u \times N_v$ grid defined by parameters $u_i = (i-1)/(Nu-1)$ and $w_j = (j-1)/(Nw-1)$. These parameters are used to obtain points in $\mathcal{LV}^0$ (material points) by evaluating Ψ^0.

Myocardial points at positive times, X_{ij}^t, are obtained by iteratively applying the deformation maps, V^t, between two consecutive frames:

$$X_{ij}^t = \begin{cases} X_{ij}^0 = \Psi^0(u_i, w_j) & t = 0 \\ X_{ij}^t = X_{ij}^{t-1} + V^{t-1}(X_{ij}^{t-1}), & t > 0 \end{cases}$$

The mapping Ψ^t is the minimum of a cost functional of the form (3) given by changing X_{ij}^0 for X_{ij}^t. Notice that by keeping the same initial parameters, (u_i, w_j), for the spatial points, the parametric domain Ω remains the same for all times.

4 REGIONAL ANALYSIS OF THE LV FUNCTION

In order to explore left ventricular dynamics, the vectorial data provided by HPF is mapped into the normalized domain Ω. Unlike scalar data, that can be directly mapped to Ω (via Ψ^t), displacement vectors are expressed in image coordinates. These global coordinates depend on the acquisition conditions prone to vary across patients. In order to get intrinsic coordinates, vectorial data should be expressed in terms of the local references associated to the $\mathcal{LV}$ parametrization. Instead of using the Jacobian of the inverse map, we decompose (Spivak, 1999) vectors into their circumferential (corresponding to the u coordinate) and radial (corresponding to the w coordinate) components. The coordinates of the local parametric vectors are given by the columns of the Jacobian of the mapping Ψ. We will note by $\tilde{V}^t = (\tilde{U}^t, \tilde{V}^t)$ the coordinates of the deformation vectors in the local reference system. In order to compare across patients they are mapped back to the normalized domain:

$$\mathcal{U}\Omega^t(u, v) := \tilde{U}^t(\Psi^t(u, v))$$
$$\mathcal{V}\Omega^t(u, v) := \tilde{V}^t(\Psi^t(u, v))$$

The above vector fields allow a point-wise comparison. In order to provide a more intuitive (for visual assessment) and robust (from the statistics point of view) representation of the $\mathcal{LV}$ function, we analyze data within regions. Regions in Ω are defined by giving a uniform grid. We will call grid cells along the circumferential direction sectors and those along the radial direction layers. A region division is determined by the parameters defining the cells corners. Thus, a division in N_{sec} sectors and N_{lay} layers is given by $\{(u_i, w_j)\}_{i,j=1}^{N_{sec}+1, N_{lay}+1}$, where $u_i = (i-1)/N_{sec}$ and $w_j = (j-1)/N_{lay}$. A given region, ω_{IJ}, in sector I and layer J is defined as:

$$\omega_{IJ} = \{(u, w) \in \Omega / \cdots$$
$$u_I \leq u \leq u_{I+1}, w_J \leq w \leq w_{J+1}\}$$

Regional values for the components of the displacement fields are obtained as the mean of the components inside each region ω_{IJ}. We will denote by $V\omega(I, J) = (\mathcal{U}\omega(I, J), \mathcal{V}\omega(I, J))$ a regional vector in sector I and layer J.

5 RESULTS

Our average model of the LV function has been extracted from a data set of 17 healthy volunteers, composed by 12 males and 5 females aged between 23
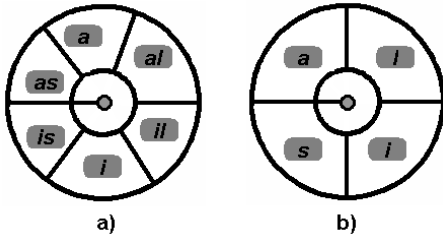
Figure 7: American Heart Association nomenclature for myocardial segments. a) Basal and mid sectors: anterior (*a*), anterolateral (*al*), inferolateral (*il*), inferior (*i*) inferoseptal (*is*) and anteroseptal (*as*). b) Apical sectors: anterior (*a*), lateral (*l*), inferior (*i*) and septal (*s*).

and 55 (31±8.3). In order to avoid misalignments due to breathing, sequences were recorded in breathhold. For the acquisition of the tagged sequences, a Siemens Avanto 1.5 T (Erlangen, Germany) equipment was used. Images have a resolution of 1.3×1.3 mm per pixel and a thickness of 6 mm per cut.

For each of the the 17 volunteers, we have considered apical (noted by *A*) and basal (noted by *B*) cuts. Our regional model is composed of 3 layers, 15 sectors and 9 equidistant stages of the systolic cycle. The normality patterns are given by the average of the 17 regional values.

$$\mathcal{UN}_l^t(I,J) = \frac{1}{17} \sum_{n=1}^{17} \mathcal{U}\omega_{l,n}^t(I,J)$$
$$\mathcal{VN}_l^t(I,J) = \frac{1}{17} \sum_{n=1}^{17} \mathcal{V}\omega_{l,n}^t(I,J)$$

where $I = \{1, \cdots, 3\}$, $J = \{1, \cdots, 15\}$, $l = \{B, A\}$ and $t = \{1, \cdots, 9\}$ and they stand for layers, sectors, levels and times, respectively.

The values obtained are showed in fig.8 for the basal model and fig.9 for the apical one. In order to provide a clearer and more intuitive model, functional values are shown as arrows in a bull's eye graphic divided into 3×15 regions. For each model we show the dynamical behavior in the 9 stages (given in percentages) of the systolic cycle. The arrows of each region show the trend of the deformation, while the color of the region codifies its magnitude (in pixels) that is specified by the color bar shown in the right. The bold line corresponds to the V_x of our affine reference defined in Section 3.1. Although we have considered a higher number of sectors, we will use the nomenclature of the American Heart Association (Cerqueira and et al., 2002) (depicted in figure 7) for referencing them in the subsequent explanations.

From the graphics in fig.8, we can appreciate that at basal levels the *a* and *al* sectors start to contract while the rest present a counterclockwise rotation.

From 37.5% of the systole to the end, all sectors rotate clockwise, though *a*, *al* and *il* sectors also experiment some contraction. Concerning apical levels (fig.9), at begin systole they experience a counterclockwise rotation for all sectors but for the *i*. At 12.5% of the systolic cycle, the sectors *s* and *i* start to contract strongly while the remaining continues rotating counterclockwise until 50%. From this stage on, sectors *s* and *i* also present some clockwise rotation, while the remaining keep the same rotational tendency.

We have also explored whether the sectorial tendency observed in the bull's eye graphics is consistent with the anatomical disposition of the ventricular band segments (fig2). On a given ventricular band segment, fiber orientation keeps approximately constant (Torrent-Guasp et al., 2005). It follows that regional motion should be similar on sectors belonging to the same ventricular band segment. In order to verify such condition we have considered the regional motion for the whole sequence described by the motion vectors for all times:

$$\mathcal{UN}_l(I,J) = (\mathcal{UN}_l^1(I,J), \ldots, \mathcal{UN}_l^9(I,J))$$
$$\mathcal{VN}_l(I,J) = (\mathcal{VN}_l^1(I,J), \ldots, \mathcal{VN}_l^9(I,J))$$

The set $(\mathcal{UN}_l(I,J), \mathcal{VN}_l(I,J))$ provides a feature space for the regional motion of 18 dimensions. We have performed a 2-class unsupervised clustering to search for areas of uniform motion. We note that, since the main motions of cardiac tissue are rotation and contraction, the clusters detect contractile and rotational areas.

The sequence regional motion clusters for base and apex are given in fig.10.a and .b, respectively. On top we have the colored segments of the bovine heart and on bottom the classification of the bull's eye regions. The angular origin is depicted in all images in solid bold line. The classification output is stamped on the colored myocardium in double line ellipses. Firstly we note that the regions of homogenous motion are consistent with the visual assessment of fig.8 and 9. Secondly, areas of uniform motion present a good correlation with the division given by the ventricular band segments. Mismatches (especially at segment borders) are attributed to anatomical variability across species.

6 CONCLUSIONS AND FUTURE WORK

In this paper we introduce a novel approach for exploring the regional dynamics of the left ventricle. We
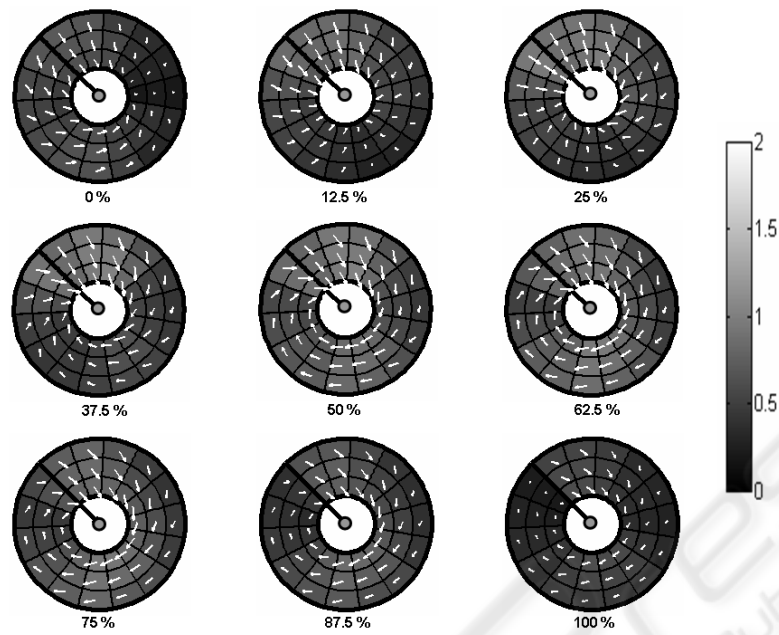
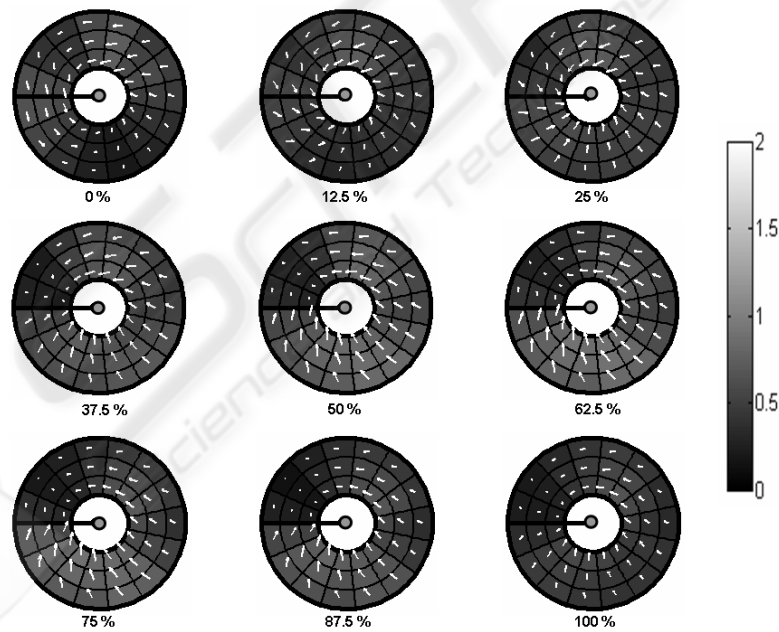Figure 8: Regional Normality Patterns for Basal Level.

Figure 9: Regional Normality Patterns for Apical Level.

provide a general framework for computation of normality patterns and compute regional patterns from healthy subjects. Our experiments prompt two relevant issues. Firstly, motion is not uniform for a given cut, so that, for a proper localization of the lesion, a regional approach is more suitable than using global scores (such as rotation or torsion (Garcia et al., 2006; Lorenz et al., 2000)). Secondly, there is a strong relation between regional variability in heart motion and the disposition of the ventricular band in space. The promising results obtained for the 2D case encourage extending the methodology to three dimensions.
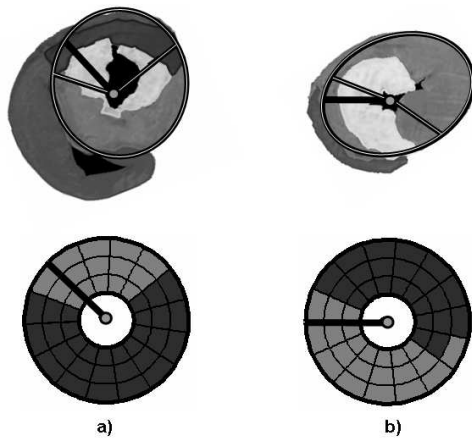
Figure 10: Correlation between ventricular band anatomy (of a bovine heart) and uniform regional motion (of healthy humans) for base a) and apex b).

ACKNOWLEDGEMENTS

REFERENCES

Axel, L. and Dougherty, L. (1989). Mr imaging of motion with spatial modulation of magnetization. *Radiology*, 171:841–845.

Cerqueira, M. and et al. (2002). Standardized myocardial segmentation and nomenclature for tomographic imaging of the heart. *Circulation*, 105:539–542.

Chandrashekara, R., Rao, A., Sanchez-Ortiz, G. I., Mohiaddin, R. H., and Rueckert, D. (2003). Construction of a statistical model for cardiac motion analysis using nonrigid image registration. In *Proc. IPMI*.

Garcia, J., Gil, D., Barajas, J., Carreras, F., Pujades, S., and Radeva, P. (2006). Characterization of ventricular torsion in healthy subjects using gabor filters in a variational framework. In *IEEE Proceeding Computers in Cardiology*.

Garot, J., Blumke, D., Osman, N., Rochitte, C., McVeigh, E., and Zerhouni, E. (2000). Fast determination of regional myocardial strain fields from tagged cardiac images using harmonic phase mri. *Circulation*, 101(9):981–988.

Gotte, M., Germans, T., Russel, I., Zwanenburg, J., Marcus, J., van Rossum, A., and van Veldhuisen, D. (2006). Myocardial strain and torsion quantified by cardiovascular magnetic resonance tissue tagging: Studies in normal and impaired left ventricular function. *J. A. Coll. Cardiology*, 48(10):2002–2011.

Guttman, M., Prince, J., and McVeigh, E. (1994). Tag and contour detection in tagged mr images of the left ventricle. *Medical Imaging, IEEE Transactions on*, 13(1):74–88.

Horn, B. and Schunck, B. (1981). Determining optical flow. *Artificial Intelligence*, 17:185–204.

Jung, B., Kreher, B. W., Markl, M., and Henning, J. (2006). Visualization of tissue velocity data from cardiac wall motion measurements with myocardial fiber tracking: principles and implications for cardiac fibers structures. *European Journal of Cardio-Thoracic Surgery*, 295:158–164.

Kocica, M., Corno, A., Carreras-Costa, F., Ballester-Rodes, M., Moghbel, M., Cueva, C., Lackovic, V., Kanjuh, V., and Torrent-Guasp, F. (2006). The helical ventricular band: global, three-dimensional, functional achitecture of the ventricular myocardium. *European Journal of Cardio-thoracic Surgery*, 29:S21–S40.

Li, J. and Denney, T. (2006). Left ventricular motion reconstruction with a prolate spheroidal b-spline model. *Phys. Med. Biol.*, 51:517–537.

Lorenz, C., Pastorek, J., and Bundy, J. (2000). Delineation of normal human left ventricular twist troughout systole by tagged cine magnetic resonance imaging. *J Cardiov. Magn. Reson.*, 2(2):97–108.

Luo, G. and Heng, P. (2005). Lv shape and motion: B-spline-based deformable model and sequential motion decomposition. *IEEE T Inf. Technol. B.*, 9(3):430–446.

Osman, N. F., Kerwin, W. S., McVeigh, E. R., and Prince, J. L. (1999). Cardiac motion tracking using cine harmonic phase (harp) magnetic resonance imaging. *Magnetic Resonance in Medicine*, 42:1048–1060.

Rao, A., Sanchez-Ortiz, G., Chandrashekara, R., Lorenzo-Valdes, M., Mohiaddin, R., and Rueckert, D. (2003). Construction of a cardiac motion atlas from mr using non-rigid registration. In *Functional Imaging and Modeling of the Heart*.

Spivak, M. (1999). *A Comprehensive Introduction to Differential Geometry, vol. 1 (3rd edition)*. Publish or Perish, Inc.

Torrent-Guasp, F., Kocica, M., Corno, A., Komeda, M., Carreras-Costa, F., Flotats, A., Cosin-Aguilar, J., and Wen, H. (2005). Towards a new understanding of the heart structure and function. *European Journal of Cardio-thoracic Surgery*, 27:191–201.

Waldman, L., Nosan, D., Villarreal, F., and Covell, J. (1988). Relation between transmural deformation and local myofiber direction in canine left ventricle. *Circ. Res.*, 63 (3):550–62.

Zerhouni, E., Parish, D., Rogers, W., Yang, A., and Shapiro, E. (1988). Human heart: tagging with mr imaging–a method for noninvasive assessment of myocardial motion. *Radiology*, 169(1):59–63.

Zitova, B. and Flusser, J. (2003). Image registration methods: A survey. *Im. Vis. Comp.*, 21:977–1000.